Role of electron wavepacket interference in the optical response of helium atoms

PAPER • OPEN ACCESS

Role of electron wavepacket interference in the optical response of helium atoms

New Journal of Physics
The open access journal for physics

Role of electron wavepacket interference in the optical response of helium atoms

Matteo Lucchini[1], **Jens Herrmann, André Ludwig, Reto Locher, Mazyar Sabbar, Lukas Gallmann and Ursula Keller**

Department of Physics, Institute of Quantum Electronics, ETH Zurich, CH-8093 Zürich, Switzerland
E-mail: mlucchini@phys.ethz.ch

New Journal of Physics **15** (2013) 103010 (15pp)
Received 23 May 2013
Published 8 October 2013
Online at http://www.njp.org/
doi:10.1088/1367-2630/15/10/103010

Abstract. Attosecond control of the optical response of helium atoms to extreme ultraviolet radiation in the presence of moderately strong infrared laser light has been recently demonstrated both by employing attosecond pulse trains (APTs) and single attosecond pulses. In the case of APTs the interference between different transiently bound electron wavepackets excited by consecutive attosecond light bursts in the train was indicated as the predominant mechanism leading to the control. We studied the same physical system with transient absorption spectroscopy using elliptically polarized infrared pulses or APTs with a varying number of pulses down to a single pulse. Our new results are not consistent with this kind of wavepacket interference being the dominant mechanism and show that its role in the control over the photoabsorption probability has to be rediscussed.

[1] Author to whom any correspondence should be addressed.

Contents

1. Introduction

Fundamental mechanisms initiated by the absorption of light photons are known to happen on an ultrafast time scale. In the last few decades, the development of attosecond science has provided a new tool to investigate these phenomena. Despite the important steps made [1], a complete understanding of the light–matter interaction is still missing even in the case of simple systems. A remarkable example is the photoabsorption and photoionization of helium (He). In 2007 Johnsson *et al* [2] applied an attosecond pulse train (APT) in combination with a synchronized few-cycle infrared (IR) field in a pump–probe scheme, to study the photoionization of He around its first ionization threshold. The authors demonstrated the possibility to control the ionization probability on an attosecond time scale by changing the relative delay between the APT and the IR pulse. They observed a sinusoidal oscillation of the ionization probability as a function of delay. This modulation was explained with two main mechanisms: (i) distortion of the atomic potential induced by the IR field and (ii) interference of electron wavepackets (EWPs) created by subsequent pulses of the APT (see figure 1). The calculations performed by the authors suggested that the EWP interference is predominant. Therefore a reduction of the number of attosecond pulses in the train should lead to a strong reduction of the oscillation contrast. In particular only a weak modulation of the ionization and photoabsorption probabilities should be observed if single attosecond pulses (SAPs) instead of APTs are employed to excite the system.

The delay-dependent modulation of the photoabsorption/photoionization probability was further investigated both theoretically [3] and experimentally [4] showing that the temporal (or spectral) features of the APT have an influence on the process. A few years later Holler *et al* [5] obtained further evidence for this picture by the investigation of the complementary absorption probability with transient absorption (TA) spectroscopy. As an all-optical technique, TA consists in detecting the transmitted XUV spectra as a function of the relative APT—IR pulse delay rather than the ionization fragments [5, 11, 12]. Thus, it is also able to probe the behavior of bound states, which are not directly accessible with conventional attosecond spectroscopy techniques.

In the case of SAP excitation of the IR-laser dressed helium, sub-cycle control over the photoelectron emission has been demonstrated [8]. The observed IR-induced oscillations of the photoelectron spectrum was attributed to a ‘which way’ interference between direct XUV excitation and an IR-assisted two-color transition (see figures 1(b) and (c)). The complementary optical response of helium exposed to a SAP has recently been investigated with the TA technique both experimentally [6, 7, 9] and theoretically [10].

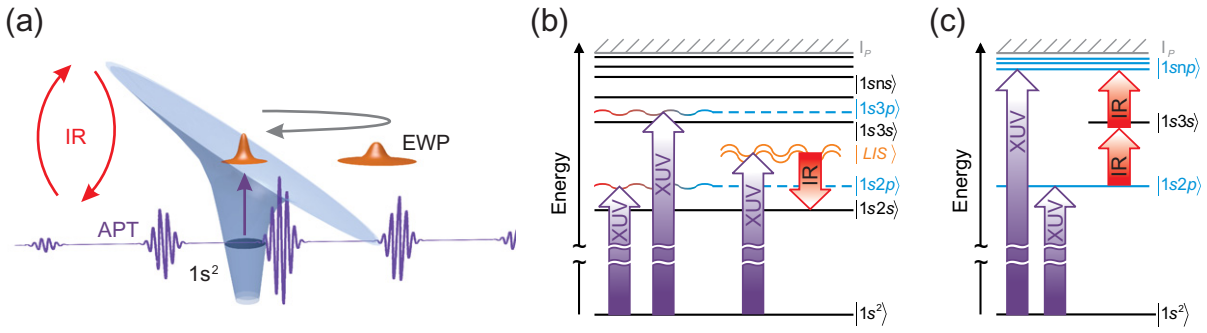

Figure 1. Schematic of the main mechanisms proposed to explain the oscillation of the photoabsorption probability in the case of APT (a) and SAP excitation (b)–(c). (a) Interference between two parts of a transiently bound EWP excited by subsequent pulses in the APT [2, 5]. (b) Resonant absorption lines of the 1s*n*p series affected by sub-cycle ac Stark shift and light-induced structures associated with two-photon/two-color processes [6, 7]. IR dressed states are represented with wavy lines. (c) 'Which way' interference between direct extreme-ultraviolet (XUV) excitation and an IR-assisted two-color transition [8–10].

In this paper we address a few remaining open questions: how does the system behave during the transition from multiple to SAP excitation? How strong is the modulation of the photoabsorption probability affected by the interference mechanisms initiated within the same attosecond pulse compared to the wavepacket interference generated by subsequent attosecond pulses?

We employed APTs in a TA experiment in order to find an answer to these questions. In the second section we will present the results obtained by changing the time duration of the driving IR pulses used in the high-order harmonics generation (HHG) process, i.e. by effectively changing the number of pulses in the APT. We will demonstrate that the oscillation strength is unexpectedly insensitive to the number of attosecond pulses interacting with the He atoms. As further evidence we will present and discuss in section 3 the results obtained by a direct comparison of the oscillation strength observed in the regimes of single and multiple attosecond pulses. The interference mechanism requires the transiently bound EWP to be in the proximity of the nucleus when the next attosecond pulse interacts with the atom. Therefore a strong dependence on the polarization of the external IR field used in the pump–probe experiment is expected. IR fields with a large ellipticity will effectively prevent the transiently bound EWP from returning to its parent ion. The experimental dependence of the oscillation strength on the degree of ellipticity of the few-femtosecond IR pulses presented in section 4 agrees only partially with the predictions. Finally, section 5 contains the conclusions.

2. Dependence on the attosecond pulse train time duration

The EWP interference picture proposed in [2] to explain the fast oscillation of the ionization probability of He is based on the assumption that two parts of an EWP excited by subsequent attosecond pulses of the train can interfere. Moreover, it was predicted that also the photoabsorption probability should oscillate with half the period of the IR field used in

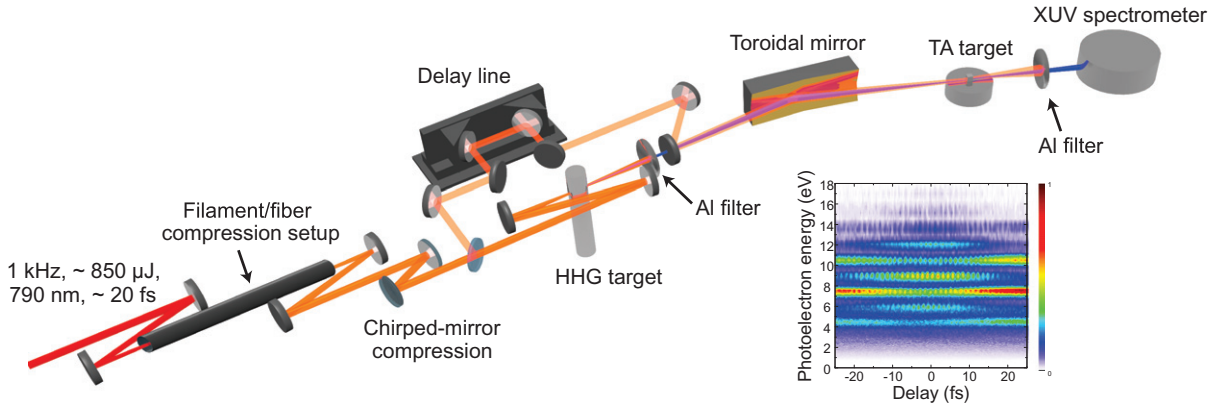

Figure 2. Schematic of the experimental setup. The inset shows a RABBITT trace [13] obtained with the APTs employed in the experiment. Few-cycle pulses are generated starting from 850 μJ IR pulses with a time duration of $\sim$20 fs and a central wavelength of 790 nm by means of the filamentation or hollow-core fiber pulse compression technique. The IR beam is subsequently divided into two arms by a beamsplitter. The more intense part of the beam is used to generate the harmonics. The delay of the remaining IR pulse is adjusted before being recombined with the XUV light. The two beams are then focused by a gold-coated toroidal mirror into a pulsed He gas target (TA target). The transmitted spectrum is recorded by an XUV spectrometer after removal of the residual IR light with a second aluminum filter.

the pump–probe scheme. As the authors showed in their calculations, the strength of the oscillations is expected to scale quadratically with the number of attosecond pulses constituting the train. This modulation of the photoabsorption probability was experimentally observed in a TA experiment [5], however its dependence on the number of attosecond pulses in the APT has never been investigated.

We adopted a scheme similar to the one in [5] and studied the fast dynamics of the photoabsorption probability as a function of time duration of the APT. The experimental setup is sketched in figure 2. Few-femtosecond IR pulses with an energy of $\sim$850 μJ and a time duration of $\sim$20 fs are further compressed either by filamentation [14] or by propagation through a hollow-core fiber filled with argon gas [15]. The IR beam is then divided into two parts by a broadband beamsplitter with a reflectivity of 20%. The transmitted part is focused into a 3 mm long cell filled with xenon gas to generate high-order harmonics (HH). After blocking the residual IR field with a 100 nm thick aluminum filter, the XUV light is recombined with the other arm of the interferometer using a mirror with a central hole. Both beams are subsequently focused by a toroidal mirror into a 1.5 mm long cell filled with He. The cell is mounted on top of a pulsed valve operating at the laser repetition rate with an opening time of $\sim$60 μs. The density of He atoms in the cell is kept constant at a value of $\sim 5 \times 10^{17}$ particles cm^{-3}. The delay between the IR and XUV beams is actively controlled by a closed-loop piezoelectric actuator, which allows a minimal step size of 107 as. At the end of the optical path an XUV spectrometer records the spectra of the transmitted light with a resolution of $\sim$50 meV in the region of interest.

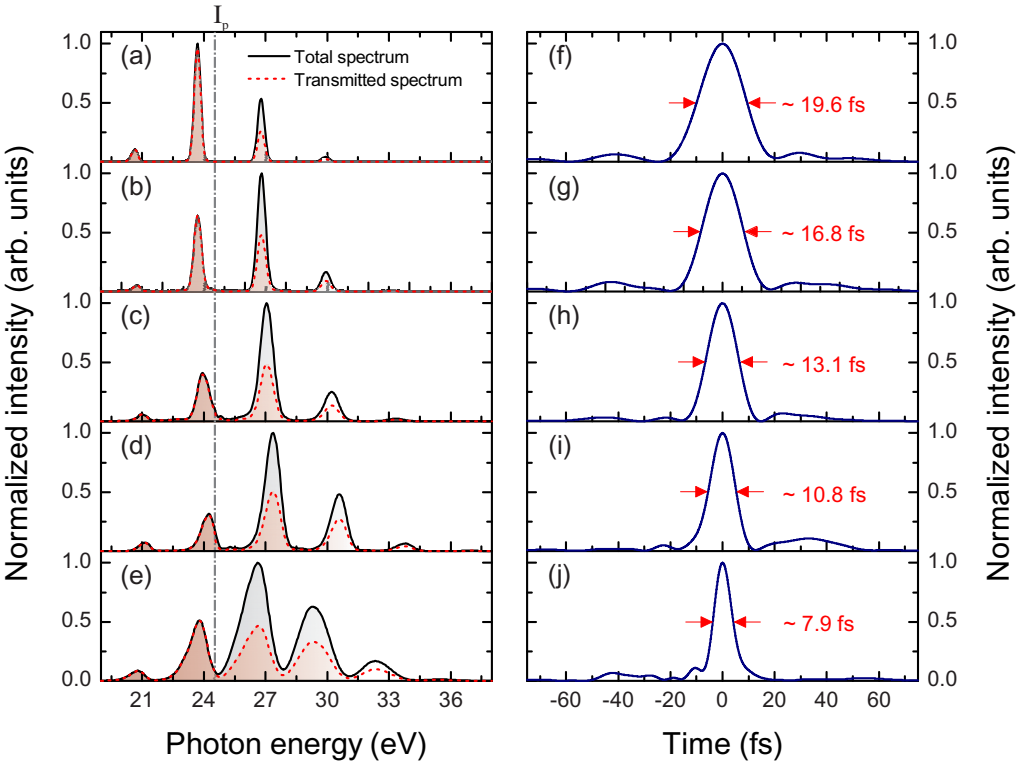

Figure 3. XUV spectra associated with the different APTs employed in the experiment. (a)–(e) Harmonic spectra (black solid lines) and, (f)–(j) SPIDER reconstructions of the IR driving pulses used to generate them. As expected, the width of the individual harmonics is inversely proportional to the time duration of the driving pulses. The red dotted curves in (a)–(e) show the transmitted spectra after absorption in the TA target filled with He gas in the absence of the IR field. The dash-dotted gray line marks the ionization potential of He, $I_p = 24.59$ eV.

For a given peak intensity, the number of attosecond pulses within the train is directly linked to the time duration of the driving IR pulse. By changing the parameters of the IR pulse compression setup it is possible to tune the time duration of the driving pulses and so the duration of the associated APT. Figure 3 shows the HHG spectra (left panels, black-solid curves) together with the SPIDER [16] measurements of the IR driving pulses used for their generation (right panels). The width of each harmonic in the comb is inversely proportional to the time duration of the APT. Indeed, the experimental XUV spectra show that the bandwidth of the harmonics increases with a decreasing duration of the generating pulse (see figure 4(c)). The spectra from figures 3(a)–(d) were obtained with the filament compression setup, while the 7.9 fs IR driving pulses of figure 3(j) were generated with the hollow-core fiber setup. A rough estimate of the number of pulses constituting the train in each case can be obtained by calculating the harmonic spectrum generated by the driving IR fields measured with SPIDER. We calculated the single-atom response by using the non-adiabatic saddle-point model adapted for a numerically defined driving pulse [17]. The simulations reveal that the number of attosecond pulses having an intensity higher than 1% of the APT peak intensity goes from a maximum of 16 pulses in the case of the 19.6 fs driving pulse to 7 for the shortest APT employed (see figure 4(d)).

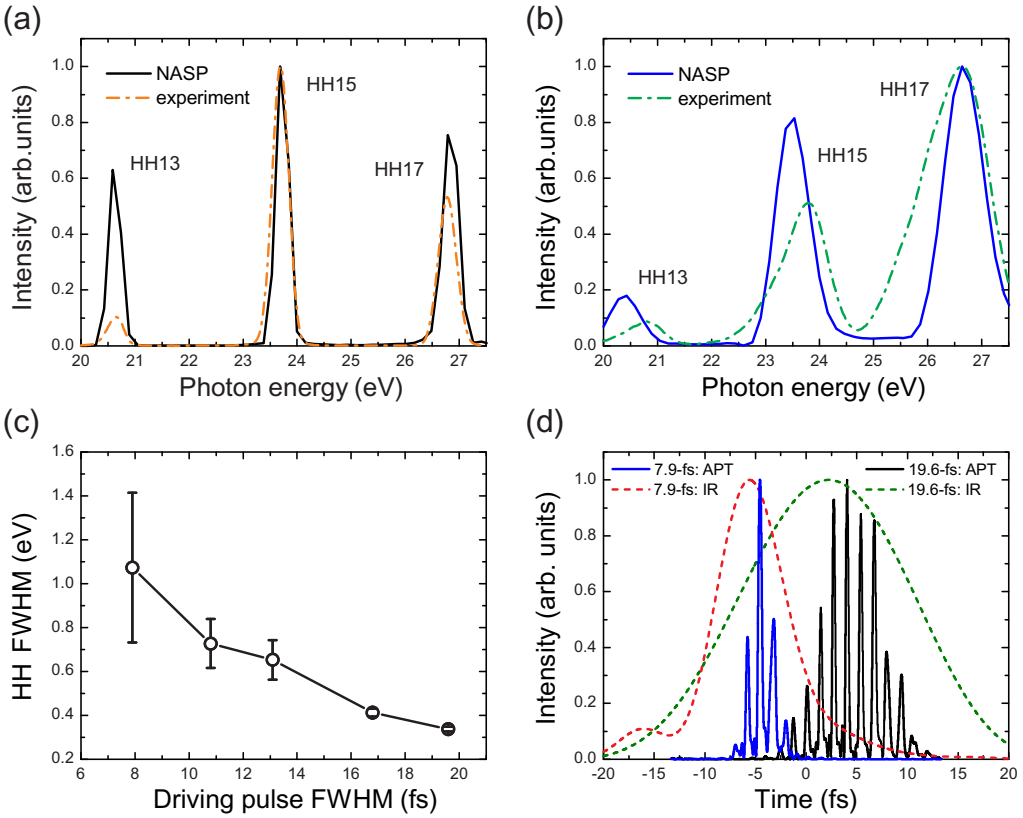

Figure 4. Single-atom response calculated with the non-adiabatic saddle-point approximation starting from the SPIDER-retrieved electric fields of figure 3. (a), (b) Comparison between calculated and experimental harmonic spectra for the 19.6 and 7.9 fs IR driving pulses of figures 3(f) and (j), respectively. (c) Experimental mean full-width half-maximum (FWHM) of the HH in figures 3(a)–(e) as a function of the driving pulse time duration. The error bars are defined as $\pm\beta$ where 2β represents the FWHM of the Gaussian distribution. (d) APTs (solid curves) associated to the calculated spectra in (a) and (b). The dashed curves show the corresponding envelope of the IR driving pulses used in the calculations. In order to match the experimental conditions, the intensity of the IR pulse was set to $1.75\times10^{14}\,\mathrm{W\,cm^{-2}}$ and only the contribution of the so-called short trajectories was taken into account [18].

For each APT of figure 3 we performed a TA measurement recording the transmitted XUV spectra as a function of the delay of the APT with respect to the IR pulse. Changing the time duration of the APT in our experimental arrangement implies that the time duration of the IR pulses used in the pump–probe scheme changes accordingly. Therefore we adjusted the power of the IR pulses in order to keep the peak intensity in the interaction region fixed to a value of $\sim2.8\times10^{12}\,\mathrm{W\,cm^{-2}}$. Figures 5(a)–(c) show the results obtained for driving pulse durations of 19.6, 13.1 and 7.9 fs, respectively. The optical response exhibits a complex behavior that becomes richer for shorter APTs. Nevertheless, clear oscillations with half the period of the IR laser field are present in the vicinity of the harmonic peaks for all three cases.

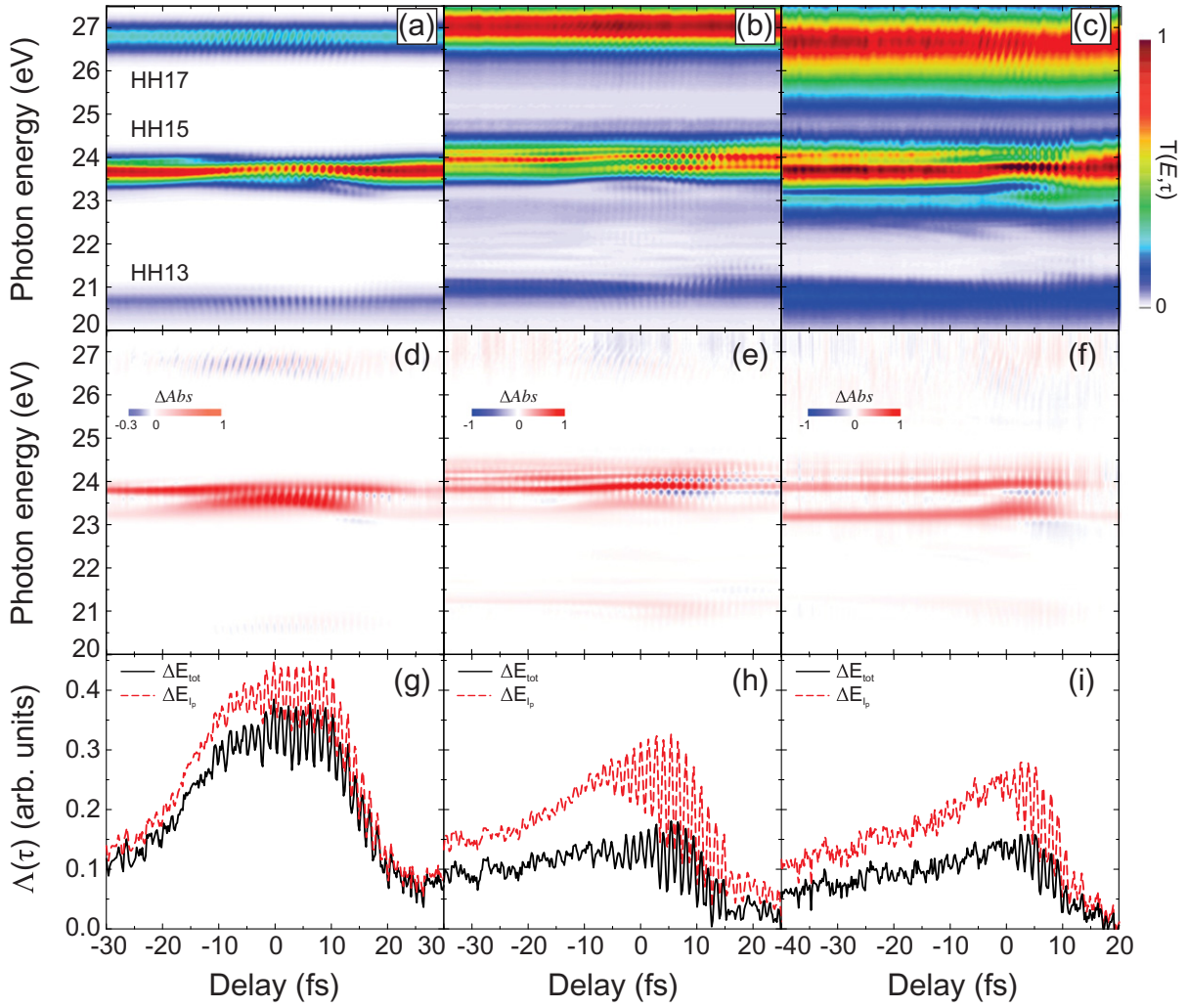

Figure 5. (a)–(c) Raw transmitted XUV spectra measured with the APTs represented by the HHG spectra displayed in figures 3(a), (c) and (e), respectively. (d)–(f) Corresponding TA signal $\Delta\mathrm{Abs}(\tau)$. (g)–(i) Energy-integrated normalized absorption $\Lambda(\tau) = \Delta\mathrm{Abs}(\tau)/T_0$ defined in equation (1), for the full energy integration window $\Delta E_{\mathrm{tot}} = [20\,\mathrm{eV}, 27.5\,\mathrm{eV}]$ (black-solid curves) and for the region below the ionization threshold I_{p}, $\Delta E_{I_{\mathrm{p}}} = [20\,\mathrm{eV}, I_{\mathrm{p}}]$ (red-dashed curves). Clear oscillations with half the period of the IR field are present in both the energy-resolved and energy-integrated data.

In order to compare the oscillation contrast of different measurements, we calculated the IR-induced absorption $\Delta\mathrm{Abs}(E, \tau)$ as equal to $-\Delta T(E, \tau) = T_0(E) - T(E, \tau)$, where $T(E, \tau)$ is the transmitted XUV spectrum with the IR pulse delayed by τ with respect to the APT. $T_0(E)$ is the transmitted spectrum when the external IR field is turned off. The $\Delta\mathrm{Abs}(E, \tau)$ associated with the TA scans of figures 5(a)–(c) are shown in figures 5(d)–(f), respectively. The IR-induced features of $\Delta\mathrm{Abs}(E, \tau)$ are confined to an energy window between 20 and 27.5 eV for all investigated cases. The strongest change in absorption is found around the 15th harmonic. The XUV photons belonging to this harmonic lie just below the ionization potential

$I_p = 24.59\,\text{eV}$. When no external IR field is present only weak absorption is recorded due to the excited states accessible through single-photon transitions in this energy region. If the IR field is turned on, two-photon transitions into the continuum become possible. The atom can absorb an XUV photon together with an IR photon and have enough energy to overcome the I_p. This process leads to an enhancement of absorption when the two pulses are temporally overlapping and the probability for a two-photon/two-color transition is higher.

Our goal is to quantitatively compare the observed modulation contrast for an energy window of interest ΔE. As clearly shown in figure 3, different time durations of the driving IR pulse correspond to substantially different XUV spectra, which complicates this task. To address this, we normalize $\Delta\text{Abs}(E, \tau)$ with respect to $T_0(E)$ and define the energy-integrated normalized absorption $\Lambda(\tau)$ as follows:

$$\Lambda(\tau) = \frac{\Delta\text{Abs}(\tau)}{T_0} = -\frac{\int_{\Delta E}[T(E,\tau) - T_0(E)]\,\mathrm{d}E}{\int_{\Delta E} T_0(E)\,\mathrm{d}E}. \quad (1)$$

Figures 5(g)–(i) show $\Lambda(\tau)$ integrated over the full energy window of interest $\Delta E_{\text{tot}} = [20\,\text{eV}, 27.5\,\text{eV}]$ (black-solid curves) or for energies just below the ionization potential of He, $\Delta E_{I_p} = [20\,\text{eV}, I_p]$ (red-dashed curves). This analysis shows that, both, the absorption enhancement around $\tau \simeq 0$ and the 2ω-oscillations (ω being the driving frequency of the IR field), are not canceled out after the energy integration process. Furthermore, when comparing the black and red curves in figures 5(g)–(i) it is possible to recognize the same main features for both investigated energy domains ΔE_{tot} and ΔE_{I_p}. This suggests that the structure of the energy-integrated signal is dominated by the optical response of the states below I_p.

In order to determine the maximum strength of the fast oscillations, we performed a Gabor time–frequency analysis of $\Lambda(\tau)$ [19]. The width of the Gaussian window function was set to 3.45 fs (~1.3 optical cycles of the IR field). The oscillation amplitude was then estimated by taking the maximum of the transformed signal located at the modulation frequency 2ω. Figure 6(a) shows the dependence of the oscillation amplitude on the APT duration. The oscillation strengths are normalized to the case of the longest APT adopted in the experiment (driving pulse FWHM = 19.6 fs). In contrast to the expectations from the EWP interference model discussed so far [2], it is found that the oscillation amplitude stays essentially constant when reducing the number of pulses in the APT (see figure 6(a)). This suggests that the picture based on the interference of EWPs excited by subsequent attosecond pulses is at least insufficient to fully explain the oscillation observed in the energy-integrated optical response of He.

Another important parameter in the experiment is the intensity of the external IR field. We performed a series of TA measurements where we changed the intensity of the IR pulse from 1.1 to $3.4 \times 10^{12}\,\text{W cm}^{-2}$ but kept the APT unchanged (see figure 6(b)). In this case a linear dependence of the oscillation amplitude on the IR pulse intensity was observed independent of the duration of the APT used in the experiment.

3. Single attosecond pulses

Further investigation of the physical mechanism at the basis of the observed 2ω-oscillations of the optical response can be obtained by employing SAPs instead of APTs. In this way any contribution ascribable to the interference of EWPs created by subsequent XUV pulses certainly is excluded. We generated SAPs both in xenon and argon gas using the polarization gating (PG) technique [20, 21] in combination with sub-6-fs IR pulses obtained with filament compression.

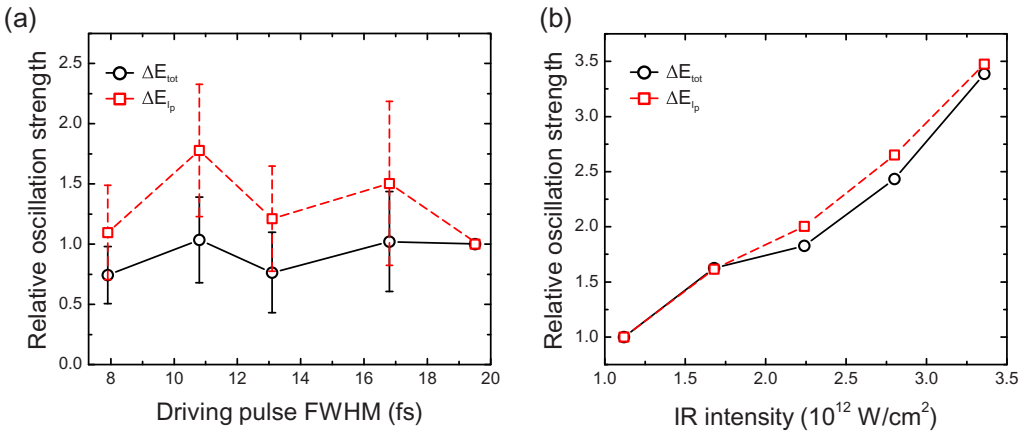

Figure 6. Evolution of the oscillation strength (a) as a function of the number of attosecond pulses composing the train and (b) as a function of the IR pulse intensity with a fixed APT (figure 3(d)). In both panels the black-solid curves refer to the full energy integrated signal ΔE_{tot}, red-dashed curves to the region below the ionization potential $\Delta E_{I_{\mathrm{p}}}$. In (a) the signal is normalized to the oscillation amplitude measured with the longest APT (driving pulse FWHM of 19.6 fs). In (b) the signal is divided by the oscillation strength obtained with an IR intensity of $\sim 1.1 \times 10^{12}\,\mathrm{W\,cm^{-2}}$. The relative oscillation strength displays a linear behavior with the IR intensity while no significant reduction of the modulation contrast is observed when using shorter APTs. The IR pulse intensities were estimated by measuring the power, the spatial intensity profile of the beam in the focus and the temporal pulse shape reconstructed by the SPIDER measurements reported in figure 3. The definition for the error bars is the same as introduced in figure 4.

The spectra of the SAP generated in argon are characterized by a FWHM of ∼9 eV with a central energy of ∼35 eV and a long spectral tail extending below 20 eV. When xenon gas is used as generating medium, the spectrum of the SAPs is centered around 27.5 eV with a FWHM of ∼5 eV (see figure 7(b)). The attosecond pulses have been fully characterized by means of the FROG-CRAB method [22]. The retrieved time duration of the SAP after 80.000 iterations of the reconstruction algorithm [23] was 410 ± 5 and 285 ± 5 as for xenon and argon, respectively. Even if the central energy and the bandwidth of the XUV spectra are different in the two cases, no appreciable changes are observed in the results.

One of the key points of the PG technique is the requirement for a stable CEP of the driving pulses. When the gate is activated, both the amplitude and shape of the generated XUV spectra show a periodic dependence on the CEP (see figure 7(a)). In particular, by changing the value of the CEP by $\pi/2$ it is possible to select XUV light characterized by a continuous spectrum (SAP generation) or by a discrete one (corresponding to the generation of two or more attosecond pulses) [24]. This enables us to perform our TA experiment and compare the optical response of He to a SAP (CEP = φ_0) or multiple attosecond pulses (CEP = $\varphi_0 + \pi/2$) without changing any other parameters of the experiment or the alignment of the beams.

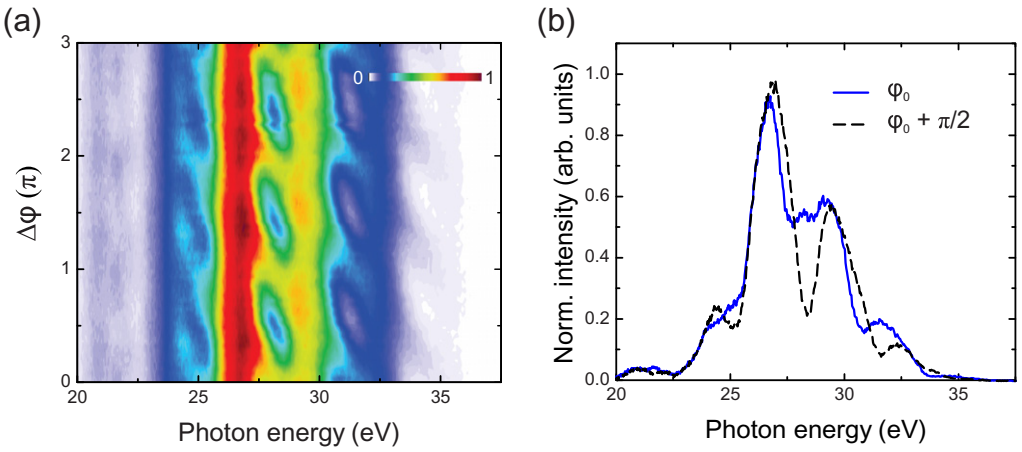

Figure 7. (a) Evolution of the XUV spectra generated in xenon with the PG technique as a function of the carrier-envelope phase (CEP) φ. (b) Line-out of the XUV spectra of (a) for two values of the CEP corresponding to a continuous (φ_0) or discrete ($\varphi_0 + \pi/2$) photon spectrum.

Figure 8 shows the transmitted XUV spectra as a function of the delay with respect to the IR pulse for SAP (figures 8(a) and (c)) or multiple attosecond pulses (figures 8(b) and (d)) generated in xenon and argon. Clear 2ω-oscillations of the transmitted spectra are observed in all the experimental traces independently of the medium adopted for the XUV light generation and from the number of attosecond pulses. The optical response of He atoms exposed to a SAP in the presence of a dressing IR laser field has been recently experimentally observed [9] and theoretically investigated [10]. The main features of the delay-dependent TA spectra have been understood in terms of: (i) resonant absorption lines of the 1s*n*p atomic states affected by sub-cycle ac Stark shift [6]; (ii) light-induced structures associated with two-photon/two-color processes (XUV±IR) which populate a non-dipole coupled s or d state [7]; (iii) 'which way' interference [8] between the direct population of the 1s*n*p states near threshold ($n > 5$) and indirect population via a three-photon/two-color process (XUV + 2IR) involving the 1s2p state. The fingerprints of these three main mechanisms are clearly present both for the case of excitation with SAP or multiple pulses (figure 8).

The EWP interference picture discussed in the context of APTs does not apply to SAPs, but should hold for the case of double or triple attosecond pulses. From this model, one would expect to observe a significant increase of the 2ω-oscillation contrast in the energy-integrated IR-induced absorption when switching from SAP (CEP $= \varphi_0$) to multiple pulses (CEP $= \varphi_0 + \pi/2$). Moreover, a phase shift of the oscillations is expected [2]. In order to estimate the total oscillation strength, we apply the method described in the previous section and calculate the normalized absorption $\Lambda(\tau)$ according to equation (1). The results are shown in figure 9. Clear oscillations with half-cycle period are still present in the energy-integrated signal for small positive delays (IR pulse comes first) and for both energy integration windows ΔE_{tot} (figure 9(a)) and ΔE_{I_p} (figure 9(b)). The time–frequency analysis reveals that the maximum strength of the oscillation stays constant within the experimental error bars. No clear increase of the oscillation strength and no phase shift due to the presence of multiple attosecond pulses is measured. This can already be seen from a direct comparison in figure 9.

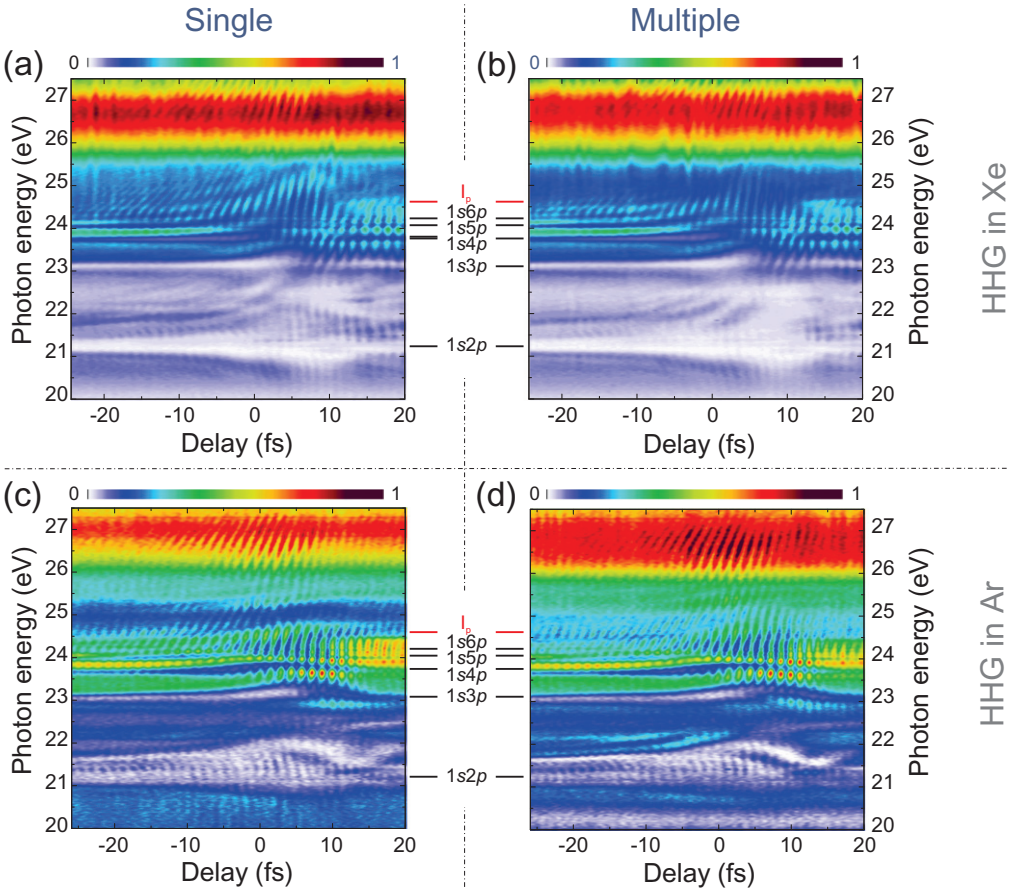

Figure 8. Delay-dependent transmitted XUV spectra for a CEP value φ_0 leading to the generation of a SAP (a, c) and for CEP = $\varphi_0 + \pi/2$ (b, d). Panels (a) and (b) are obtained with the XUV light generated in xenon while in (c, d) attosecond pulses generated in argon were employed. The lines mark the energy position of single-photon accessible atomic states of helium. Fast modulation of the transmitted signal is evident both for single and multiple attosecond pulse excitation independent of the generation medium.

As in the previous analysis, the structure of the signal integrated over the full region of interest ΔE_{tot} is mainly dominated by the response below I_{p}. In particular, the main contribution comes from the strong oscillating signal in the energy range between 24 eV and I_{p}, associated with the three-photon/two-color process, listed as point (iii) above [10]. When the XUV light arrives before the IR pulse, the fringes associated with this mechanism are expected to exhibit a clear tilt in energy [10], the reason for this being that constructive interference occurs for different delays at different energies. For positive values of the delay τ, the fringes are less tilted than for negative τ and they become almost vertical. This explains why the oscillations in the energy-integrated response $\Lambda(\tau)$ vanish for $\tau < 0$.

Another important contribution to the 2ω-oscillations of $\Lambda(\tau)$ comes from the ac Stark shift experienced by the absorption lines of the atomic states 1s3p (23.09 eV) and 1s4p (23.74 eV). As shown in figure 8, these lines exhibit a clear sub-cycle absorption oscillation which is in phase

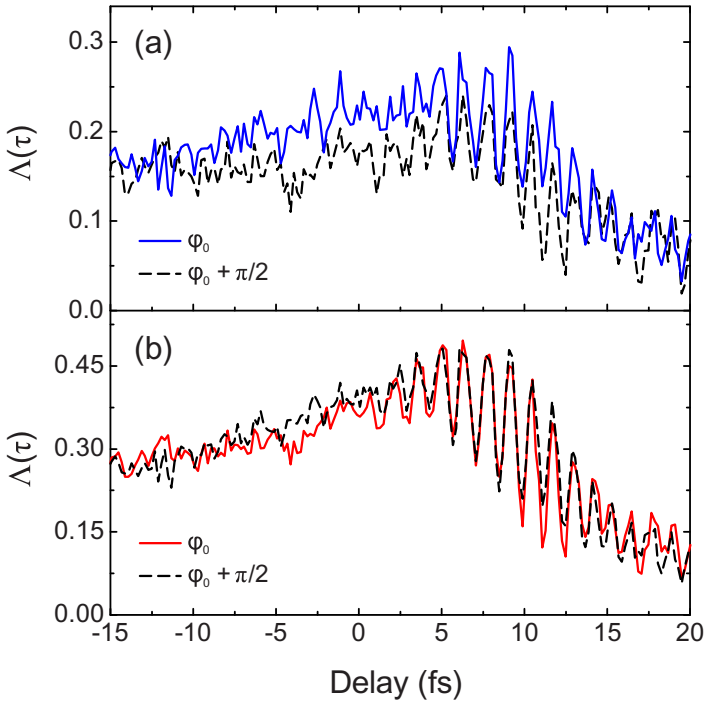

Figure 9. Energy-integrated normalized absorption $\Lambda(\tau)$, (a) for the full energy integration window $\Delta E_{\rm tot} = [20\,{\rm eV}, 27.5\,{\rm eV}]$ and (b) for the interval below the ionization threshold $\Delta E_{I_{\rm p}} = [20\,{\rm eV}, I_{\rm p}]$. In both panels, solid lines refer to the SAP of figure 8(c), black-dashed lines to the multiple-attosecond-pulse excitation of figure 8(d). Oscillations with half the period of the IR field are present for delays $\tau \geqslant 0$. No clear change in the behavior when moving from a SAP to multiple pulses is evident in the measured data.

with the signal attributed to mechanism (iii) for $\tau > 0$, thus enhancing the oscillating signal in $\Lambda(\tau)$.

4. Elliptically polarized infrared pulses

The EWP interference mechanism under investigation occurs only if some part of an initially localized wavepacket is found in the region of space where it was created when the subsequent attosecond pulse interacts with the atom. In other words, it occurs if it takes more than a half-optical cycle for the EWP to completely ionize [2]. In this time the EWP can interact with the external IR field. If so, a strong dependence of the process on the ellipticity ε of the external IR field is expected. If the IR pulse is elliptically polarized, the transient EWP will experience an additional lateral displacement as compared to the case of linear polarization, and the probability for being driven back to the parent atom decreases by several orders of magnitude for sufficiently large ε. This suppression of recollision is well known, for example, from the HHG process. The XUV generation efficiency decreases by several orders of magnitude when the ellipticity of the driving pulses increases [25, 26] (see the dash-dotted line in figure 11(b)). Indeed, this concept is at the basis of the PG technique mentioned in the previous section. The polarization of the driving pulse is modified in order to change from circular to linear and then back to circular.

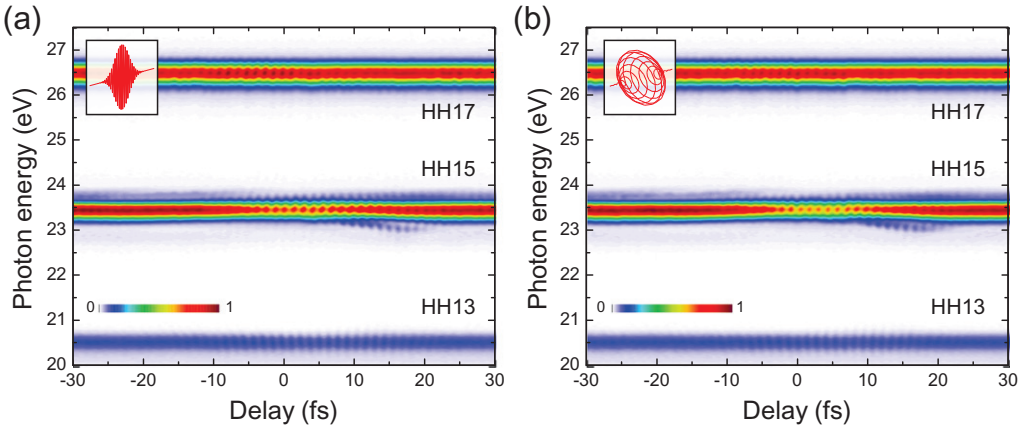

Figure 10. Delay-dependent transmitted XUV spectra for high-order harmonics generated in Xe with 20 fs IR driving pulses. (a) Linearly polarized IR pulses, (b) elliptically polarized IR pulses ($\varepsilon_{\max} = 0.66$). The 2ω-oscillations of XUV transmission of the IR-dressed He are clearly visible in both cases.

Efficient XUV-light generation occurs only in the time window in which the ellipticity ε is lower than a threshold value $\varepsilon_{\text{th}} = 0.13$ [27].

We measured the delay-dependent transmitted XUV spectra as discussed in the second section of this work, but employing IR pulses with a variable degree of polarization ε. The IR pulses have a fixed time duration of $\sim$25 fs and an intensity of $\sim 1 \times 10^{12}$ W cm^{-2}. Control of the ellipticity ε was achieved by introducing an additional achromatic quartz quarter-waveplate into the beam path. Figure 10 shows a comparison of the transmitted XUV spectra for $\varepsilon = 0$ (linearly polarized pulses, figure 10(a)) and $\varepsilon_{\max} = 0.66$ (elliptically polarized pulses, figure 10(b)). The XUV spectrum is composed of four narrow-band harmonics (harmonic orders 13–19). For both values of ε, harmonics 13–17 exhibit a strong 2ω-oscillation of the transmitted signal. Harmonic 19 lies outside the maximum energy range, ΔE_{tot}, employed in the previous analysis and no IR-induced structures are observed. As a result we will concentrate only on the first three harmonics in the following discussion. Unlike the previously presented cases, in this experiment the value of ε is freely adjustable while leaving both the IR pulse duration and the XUV spectrum unchanged. For this reason we can directly compare the transmitted signal from different measurements without the need for normalizing the data to T_0 (equation (1)). The oscillation amplitude $O(\varepsilon)$ is obtained by calculating the Fourier transform of the energy-integrated transmitted signal: $F\{\int_{\Delta E} T(E, \tau)\, \mathrm{d}E\}$.

Figure 11(a) shows the evolution of the transmitted signal integrated over a narrow energy interval ΔE centered around HH 13, 15 and 17 (upper, middle and lower panel, respectively). The width of energy interval ΔE is determined by the resolution of our XUV spectrometer and it is equal to 34, 50 and 54 meV for harmonics 13, 15 and 17, respectively. Figure 11(b) displays the associated amplitude $O(\varepsilon)$ normalized to the oscillation strength $O(\varepsilon = 0)$ found in the case of linearly polarized IR pulses. In all investigated cases, the oscillation amplitude decreases for increasing values of ε, but the observed reduction amounts to a value of only 30–40% even for maximum ellipticity $\varepsilon_{\max}$. However, in the framework of the IR-driven transient EWP picture, a reduction by several orders of magnitude is expected already for significantly lower values of ε as is found for other recollision processes [28] (see figure 11(b)). Therefore the experimental

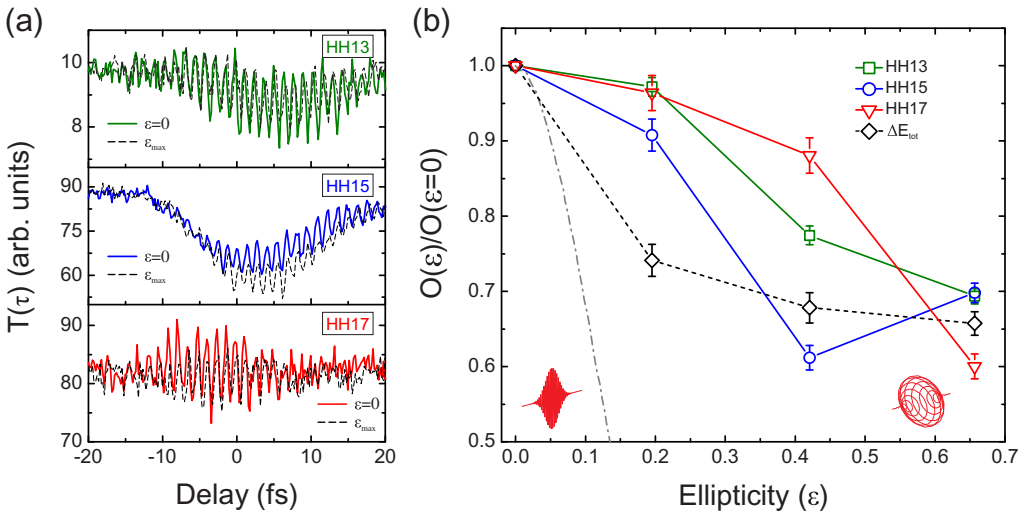

Figure 11. (a) Comparison of the delay-dependent transmission $T(\tau)$ for energy intervals centered around harmonics 13, 15 and 17 for linearly polarized (solid lines) and elliptically polarized IR pulses (dashed lines). (b) Oscillation amplitude $O(\varepsilon)$ normalized to the linearly polarized case $O(\varepsilon = 0)$. The solid colored lines have been evaluated for the same energy intervals used in (a), while the black dashed line is obtained after full energy integration of the transmitted signal ($\Delta E_{\text{tot}} = [20\,\text{eV}, 27.5\,\text{eV}]$). The gray dash-dotted line shows the relative strength of harmonic 21 generated in argon by an IR field with an intensity of $3 \times 10^{14}\,\text{W cm}^{-2}$ as calculated in [26]. A direct comparison between the well-known recollision driven process of HHG, represented by the dash-dotted line, and the experimental data shows that the two processes exhibit a complete different behavior when changing the ellipticity ε. Even though for all the cases in our experiment $O(\varepsilon)$ decreases with increasing ε, the suppression is not as strong as the one observed in the HHG process.

results confirm that the picture in which the transiently bound EWP is driven back and forth by the external IR field before interfering with another EWP is incomplete.

5. Conclusions

We studied the optical response of helium atoms excited by an attosecond pulse train and a delayed few-cycle IR pulse in a TA scheme. Clear oscillations with half the period of the IR field were observed both in the energy-resolved and energy-integrated signal. Previously it was suggested that the interference of transiently bound EWPs excited by subsequent attosecond pulses is the origin of these modulations [2]. In order to test the completeness and correctness of this model, we adjusted various relevant parameters in this experiment. We recorded the modulations for a varying number of pulses in the APT, as a function of IR intensity and ellipticity. We found that the oscillation amplitude does not scale with the number of attosecond pulses in the APT as predicted by the EWP picture. A direct comparison between the SAP and multiple-attosecond-pulses excitation showed that the strength of the oscillations is the same for both cases. Furthermore, no phase shift of the modulations is observed when switching

from APT to SAP excitation—in contrast to the theoretical predictions in [2]. Finally, further evidence on the incompleteness of the previously proposed interference mechanism is provided by the measured dependence on the ellipticity ε of the IR field. The observed scaling of the modulation contrast is not in agreement with the recollision picture implied by a transiently bound EWP being driven back and forth by the external IR field during the interaction.

To conclude, our new experimental results show that, even in the case of APTs, the interference between EWPs excited by consecutive attosecond pulses in the train is not the dominant mechanism responsible for the observed modulations of the absorption probability. The modulation of the optical density can rather be attributed to the largest extent to a 'which way' interference originating in the existence of different excitation pathways accessible through two-color interactions involving the attosecond pulses and the IR field [9, 10].

Acknowledgments

This work was supported by National Center of Competence in Research Molecular Ultrafast Science and Technology (NCCR MUST), research instrument of the Swiss National Science Foundation and by the ETH Zurich Postdoctoral Fellowship Program.

References

[1] Krausz F and Ivanov M 2009 *Rev. Mod. Phys.* **81** 163
[2] Johnsson P *et al* 2007 *Phys. Rev. Lett.* **99** 233001
[3] Rivière P, Uhden O, Saalmann U and Rost J M 2009 *New J. Phys.* **11** 053011
[4] Ranitovic P *et al* 2010 *New J. Phys.* **12** 013008
[5] Holler M, Schapper F, Gallmann L and Keller U 2011 *Phys. Rev. Lett.* **106** 123601
[6] Chini M *et al* 2012 *Phys. Rev. Lett.* **109** 073601
[7] Chen S *et al* 2012 *Phys. Rev.* A **86** 063408
[8] Mauritsson J *et al* 2010 *Phys. Rev. Lett.* **105** 053001
[9] Chini M *et al* 2013 *Sci. Rep.* **3** 1105
[10] Chen S, Wu M, Gaarde M B and Schafer K J 2013 *Phys. Rev.* A **87** 033408
[11] Goulielmakis E *et al* 2010 *Science* **320** 1614–7
[12] Wang H *et al* 2010 *Phys. Rev. Lett.* **105** 143002
[13] Paul P M *et al* 2001 *Science* **292** 1689–92
[14] Hauri C P *et al* 2004 *Appl. Phys.* B **79** 673–7
[15] Nisoli M, De Silvestri S and Svelto O 1996 *Appl. Phys. Lett.* **68** 2793–5
[16] Iaconis C and Walmsley I A 1998 *Opt. Lett.* **23** 792–5
[17] Lucchini M, Calegari F, Kim K S, Sansone G and Nisoli M 2012 *New J. Phys.* **14** 033009
[18] Salières P, L'Huillier A and Lewenstein M 1995 *Phys. Rev. Lett.* **74** 3776
[19] Gabor D 1946 *J. Inst. Elec. Eng.* **93III** 429–57
[20] Sola I J *et al* 2006 *Nature Phys.* **2** 319–22
[21] Sansone G *et al* 2006 *Science* **314** 443–6
[22] Mairesse Y and Quéré F 2005 *Phys. Rev.* A **71** 011401
[23] Kane D J 1999 *J. Quantum Electron.* **35** 421–31
[24] Sansone G *et al* 2009 *Phys. Rev.* A **80** 063837
[25] Antoine P, L'Huillier A, Lewenstein M, Salière P and Carré B 1996 *Phys. Rev.* A **53** 1725
[26] Dietrich P, Burnett N H, Ivanov M and Corkum P B 1994 *Phys. Rev.* A **50** R3585
[27] Calegari F *et al* 2012 *J. Phys. B: At. Mol. Opt. Phys.* **45** 074002
[28] Tcherbakoff O, Mével E, Descamps D, Plumridge J and Constant E 2003 *Phys. Rev.* A **68** 043804